J. Fluid Mech. (1996), *vol.* 312, *pp.* 149–172

Modelling of chemical reactions in hypersonic rarefied flow with the direct simulation Monte Carlo method

By MICHAEL A. GALLIS AND JOHN K. HARVEY

Department of Aeronautics, Imperial College of Science Technology and Medicine, London SW7 2BY, UK

(Received 27 September 1993 and in revised form 16 November 1995)

In this paper the phenomenon of chemical reactivity in hypersonic rarefied flows is examined. A new model is developed to describe the reactions and post-collision energy exchange processes that take place under conditions of molecular non-equilibrium. The new scheme, which is applied within the framework of the direct simulation Monte Carlo (DSMC) method, draws its inspiration from the principles of maximum entropy which were developed by Levine & Bernstein. Sample hypersonic flow fields, typical of spacecraft re-entry conditions in which reactions play an important role, are presented and compared with results from experiments and other DSMC calculations. The latter use traditional methods for the modelling of chemical reactions and energy exchange. The differences are discussed and evaluated.

1. Introduction

Envisaged expeditions to planets within the solar system and the requirement to improve the payload-to-weight ratio of spacecraft have revived the Apollo-era interest in the study of rarefied hypersonic flow. These vehicles travel at near orbital velocity through the upper levels of the Earth's atmosphere and the high temperatures met under such flight conditions (typically above 10000 K) provoke dissociation, chemical reactions and even ionization of the fluid through which they are travelling. The variety of real gas effects that take place substantially modify the energy flux to the vehicle. Endothermic reactions (principally oxygen and nitrogen dissociation) dominate the shock layer ahead of a re-entry vehicle and absorb energy, reducing the rise in temperature due to the comparison. Generally this leads to an alleviation of the heat transfer to the vehicle, especially if chemical recombination can be prevented from occurring on its surface through the use of non- or only slight catalytic coatings. The ceramic tiles used to cover the surface of Shuttle Orbiter were chosen for this reason. Efficient modern spacecraft design depends on having a precise understanding of the fluid dynamics, including the non-equilibrium chemical activity. Such understanding enables reliable estimates to be made of the aerodynamic heating, forces and moments that will be experienced during the re-entry. From these it should be possible to make an accurate estimation of the minimum amount of thermal protection required to maintain the vehicle's integrity.

Reliable numerical predictions of continuum high-enthalpy flow fields can be obtained using the Navier–Stokes equations. Species mass conservation equations, based on equilibrium chemical reaction rates, are coupled to these equations to provide a complete description for reacting flows. During re-entry, peak heating rates are usually experienced at very high altitude (above about 55 km) where the use of the

Navier–Stokes equations becomes questionable for several reasons. One is the inappropriateness of using a formulation based on viscosity and heat conductivity coefficients simply proportional to the gradients of velocity and temperature. These coefficients implicitly assume only a small departure of the molecular velocity distribution from that of an equilibrium gas. The combination of very rapid compressions and expansions, low densities and chemical reactions witnessed during re-entry leads to a marked degree of molecular non-equilibrium; this, in turn, gives rise to novel phenomena not seen in the continuum flows which cannot be reproduced by the Navier–Stokes equations. From a molecular viewpoint, it can be stated that when the interval between particle collisions falls to within a few orders of that associated with their transit time through the flow field, there will be insufficient interactions to achieve local equilibration of the various energy modes. Chemical reactions further perturb the thermal equilibrium by preferentially depleting some energy states while over-populating others.

The only mathematical tool available to describe such flows satisfactorily is the Boltzmann equation (see Chapman & Cowling 1972). Within this equation the state of the gas is expressed in terms of a time-dependent molecular velocity distribution function; this gives the probability at any time of a particle occupying a position in physical and velocity space. The Boltzmann equation was originally formulated for simple gases but it can be extended to include internal energy, chemical reactions and radiation by adding additional dimensions for each energy mode or chemical species. This adds considerable complexity to the equation and, even in approximated form, it is intractable for engineering applications.

An attractive and viable alternative to the direct solution of this equation is a group of numerical simulation methods. These recognize the particulate nature of the gas and describe it in terms of information (values of velocity, position, energy state, etc.) on an ensemble of sample particles (or *simulators*) that move through the computational domain, closely mimicking and representing statistically the progress of the real gas molecules. Since, even in the most rarefied cases of engineering interest, the flow contains a very large number of molecules, we are obliged to use a relatively small number of such simulators to represent the ensemble of molecules and atoms moving through the domain. The flow field is divided into computational cells to allow the status of the fluid to be monitored by spatial averaging. These simulations have proved to have enormous advantages over the direct solution to the Boltzmann equation in that they are amenable to realistic modelling of the complex chemical and energy exchange processes that take place during molecular collisions. Direct particle simulation methods are, however, computationally very demanding.

One such method that has proved especially effective is the Direct Simulation Monte Carlo method (DSMC) pioneered by Bird (see Bird 1994). In this the movement of the particles is decoupled from their collisions by advancing each of these processes alternately and independently over small equal time increments. The size of these is chosen to be significantly smaller than the local mean collision time. Candidates for inter-molecular collisions are selected from neighbouring particles in a probabilistic manner by comparing a random number with the collision probability of each pair. The outcome of each collision has to be determined using appropriate models and, for DSMC, phenomenological methods are now almost universally employed for this purpose. Probability density functions are calculated in advance for each phenomenon and the post-collision properties (velocity components, internal energies, etc.) are obtained from these by random selection. At each collision, particle pairs must also be considered for possible chemical reaction.

Although phenomenological methods have proved to be very successful, the uncertainty about the distributions of molecular velocity and internal energies that prevail in real flows has led to the adoption of an implicit local equilibrium assumption in most of the implementations of the DSMC method. Validation experiments have demonstrated that quite complex rarefied non-reacting flows can be very successfully simulated using this assumption. However, its application to chemically reacting flows, where the departure from equilibrium is considerably larger, must be regarded as dubious.

The purpose of this paper is to present a new energy exchange and chemical reaction model. Probability density functions for the post-collisions energy distributions and reactivities are derived using a maximum entropy or information theory approach. These techniques have been used for many years in the area of molecular chemistry with considerable success (Levine & Bernstein 1987). They are adapted here to take into consideration recent developments in modelling the fluid dynamic aspect of reacting flows.

2. Modelling of chemically reacting flows in DSMC computations

Bird first published a model for binary reacting collisions in 1981 (Bird 1981). He proposed that if the encounter is sufficiently energetic for a chemical reaction to occur, the reaction probability can be expressed as

$$P_r = C_1(E_c - E_a)^{C_2}\left(1-\frac{E_a}{E_c}\right)^{\zeta+3/2-\omega}, \tag{1}$$

where E_c is the total collision energy, E_a is the activation energy of the reaction and ζ is the average number of internal degrees of freedom of the two molecules. This expression is restricted to gases with coefficient of viscosity proportional to the temperature to the power ω, which can be evaluated using either Bird's (1981) variable hard sphere (VHS) or Koura & Matsumoto's (1992) variable soft sphere (VSS) collision model. The constant parameters C_1 and C_2 are determined for each reaction such that the model reproduces as well as possible the experimentally measured Arrhenius reaction rates over a prescribed temperature range. Although this model gives acceptable reaction probabilities for a near-continuum gas, being based more on considerations of mathematical tractability than physics, it has a number of significant shortcomings. The first is that the probability of many reactions does not depend on the total energy E_c, as equation (1) implies, but on the internal energy. For example, for the dissociation of nitrogen and oxygen, the reaction probabilities depend heavily on the vibrational energy of the reagents. Further disadvantages of the model are that the post-collision energy is calculated from equilibrium distributions (which is particularly inappropriate for the vibrational mode), and that the C-parameters are calculated assuming equilibrium distributions of the reagent energy. This is usually not the case in rarefied reacting flows.

The shortcomings of this model have led to a recent revision by Bird (1994) for dissociation reactions. His new model recognizes the importance of the vibrational energy in promoting these reactions and the probability is calculated as the possibility of the combined vibrational energy of the two particles overcoming the dissociation energy. Although this model addresses the energy dependence of the dissociation reactions in a physically more realistic way, the problem remains of the use of equilibrium distributions for the calculation of the post-collision energy, in particular

for the vibrational component. Unavoidably this confines the method to the near-continuum near-equilibrium regime and its applications to situations of considerable non-equilibrium becomes questionable.

Other modifications to include the effects of the vibrational energy in promoting reactions have been introduced into the original Bird model by Haas & Boyd (1993). These exhibit the same basic shortcomings as Bird's revised method.

3. Theory of energy exchange

Molecules can contain energy in the translational, vibrational, rotational and electronic modes and the exchange of energy between these produces the real gas phenomena witnessed at the macroscopic scale. For re-entry flow conditions the quantum energy states for translational and rotational are closely spaced and these modes can thus be considered as continuous distributions. However the lower vibrational energy states are more widely spaced (energy gaps are about 0.2 to 0.3 eV) and hence they should be treated as having discrete energy levels.

After a collision, whether reactive or not, the distribution of energy states is given by $P(m, E_{trans}, \Omega)\,\mathrm{d}E_{trans}\,\mathrm{d}\Omega$, where P is the probability of products occupying the internal state m (which includes vibrational, rotational and electronic excitation energy) having translational energy E_{trans} and being scattered into a solid angle in the range Ω to $\Omega+\mathrm{d}\Omega$. The post-collision energy distribution depends on the type of the interaction, the forces involved (internal and external) and the energy that the colliding partners had before the interaction. For the representation of energy exchange in DSMC computations, ideally one would treat each combination of energy levels as a separate species with its own cross-sections controlling the energy exchange during any interaction. This approach would be extremely cumbersome and impractical. As already stated, phenomenological models have been consistently adopted as a viable alternative, the most widely used being the Borgnakke & Larsen (1975) model (see also Bird 1994). After each interaction, the energy of the products is selected randomly from one of two appropriate equilibrium distributions. The translational energy is selected from the Maxwell distribution:

$$P(f_T) = \frac{\Gamma(\frac{5}{2}-\omega+\zeta)}{\Gamma(\frac{5}{2}-\omega)\,\Gamma(\zeta)}(f_T)^{3/2-\omega}(1-f_T)^{\zeta-1}, \tag{2}$$

where f_T is the fraction of translational energy in the collision products, ζ is the average number of internal degrees of freedom of the molecule and $\Gamma(\,)$ is the Gamma function. The internal energy is obtained from the Boltzmann distribution:

$$P(f_i) = \frac{\Gamma(\frac{5}{2}-\omega+\zeta_i)}{\Gamma(\frac{5}{2}-\omega)\,\Gamma(\zeta_i)}(f_i)^{\zeta_i-1}(1-f_i)^{3/2-\omega}, \tag{3}$$

where f_i is the ratio of energy in mode i to the total energy and ζ_i the number of degrees of freedom associated with this mode. Recently the Borgnakke & Larsen method has been extended by Bird (1994) to treat the vibrational energy as a distribution of discrete states.

3.1. *A maximum entropy approach to the distribution of energy states*

Even though an accurate deterministic quantum mechanics approach to solving real flows is impractical, statistical thermodynamics provides a very elegant and computationally efficient way of simulating chemical phenomena. A maximum entropy (ME) method based on these methods was pioneered by Levine & Bernstein (1987) and

this will be used here as a starting point for a new method for the determination of energy exchange and chemical reactivity in collisions. Although empirical, their method has been popular among chemists who have successfully used it for a wide variety of problems. It is worth noting that in their studies the primary interest has been the details of the chemical reaction dynamics and certain shortcomings as far as the fluid mechanics are concerned have been overlooked.

The ME method is suited to the study of binary collisions in a dilute gas at a molecular level and it is in sympathy with the statistical nature of particle simulation schemes such as the DSMC method. As will be seen, unlike all of the other methods that have been applied to reacting flows, it recognizes the particular role that each energy mode plays in the promotion of reactions and weighs its importance according to the total available energy. The necessary probability distributions required for this method to be applied to particle simulations are calculated without having to adopt the assumption of local thermodynamic equilibrium made in the other DSMC schemes.

The energy released by chemical reactions is added to the kinetic and internal energy of the products. Equal redistribution between the energy modes hardly ever appears to be realized but, in general, there is a bias towards certain modes. The way in which the energy is spread over all the possible states is referred to as the *specificity* of the distribution: if all energy states have equal probability of being occupied, the specificity of the reaction is said to be zero, but if they appear in a narrow range of states, the distribution of energy is referred to as being highly specific.

In their experimental and theoretical studies, Levine & Bernstein concluded that the post-collision energy distributions could conveniently be derived by determining their deviation from another fixed distribution which they called the *priori distribution*, P^o. For this they employed the unconditionally most probable distribution, i.e. the one obtained if all energy states available after a binary collision are equally probable. Using the principles of maximum entropy and this prior distribution, they achieved a decoupling between the statistical and dynamic contributions of each reaction. They obtained, for example, the distributions of the translational energy after a monatomic–diatomic collision as

$$P^o(f_T) = \tfrac{5}{2}(f_T)^{1/2}(1-f_T), \tag{4}$$

where f_T is the fraction of translational energy in the collision products.

In implicitly defining the prior distribution as unconditionally the most probable, Levine & Bernstein disregarded important details of collisional interaction, in particular the effect of the variable inter-molecular force. Possibly they hoped that its influence, as well as the particular behaviour associated with each chemical reaction, would be encompassed within the function determining the deviation of the prior from the actual distribution. Bird (1994) pointed out that if the prior distribution does not explicitly include the effect of the force, it is impossible to discriminate between the distribution of translational energy in the bulk gas and that of the particles that have undergone interactions. In general, these two distributions should be different (see Chapman & Cowling 1972); only for the case of the inverse-power Maxwell molecular model are the two distributions identical but this model is physically unrepresentative of most gases.† Levine & Bernstein's formulation of the prior distribution thus limits their solution to Maxwell particles, which give a poor representation of the transport

† The equilibrium distribution given by equation (2) reproduces (4) if we replace ω with its value for Maxwell particles, i.e. unity. In this case and for a monatomic–diatomic collision where the average internal degrees of freedom are 2 we get an energy dependence identical to that of equation (2).

properties of gases such as oxygen and nitrogen. It does not appear that this shortcoming can be remedied by changing the function used to calculate the deviation of the real distribution from the prior distribution.

For the application of the ME method to rarefied gas dynamics, the inclusion of an appropriate inter-molecular force model is very important since the correct representation of the viscosity and thermal conductivity is essential. The use of a prior distribution which is unconditionally the most probable one is not fundamental to the ME method and the effects of the molecular model or other external parameters (e.g. force fields that may influence the distributions) can be built into the prior distribution without any loss of generality. Since the ME method is based on quantifying the departure of the observed distributions from an equilibrium one, alternative options that can be used for the prior distributions are the Maxwellian and Boltzmann equilibrium distributions for velocity and energy respectively. These have been given in equations (2) and (3) and, by using the generalization derived by Haas, McDonald & Dagum (1993), the prior distributions can conveniently be formulated as

$$P^o(f_a) = \frac{\Gamma(\Xi_a + \Xi_b)}{\Gamma(\Xi_a)\Gamma(\Xi_b)} (f_a)^{\Xi_a - 1} (1 - f_a)^{\Xi_b - 1}, \tag{5}$$

where Ξ_a is the average number of degrees of freedom corresponding to the energy mode a (which can be vibrational, rotational or translational) and Ξ_b is the average of the remaining degrees of freedom. For the distribution of the translational energy in a collision between N particles having i internal degrees of freedom, $\Xi_a = \frac{3}{2} - \omega$ and $\Xi_b = (1/N)\sum_i \zeta_i$; this yields the Maxwellian distribution when substituted into equation (5).

3.2. *From the prior to the actual distributions*

To calculate the real distributions based on the information that the prior distributions give us about the system, we need an estimation of the deviation between the two distributions. Given a distribution of states $P(f_a)$, we can calculate the entropy associated with this as

$$S = -\sum_f P(f_a) \ln P(f_a). \tag{6}$$

The prior distribution P^o, being the most probable, maximizes the entropy of the system. At a given total energy, any other distribution will result in a lower entropy. The entropy difference between the two distributions is simply

$$\Delta S = S_{max} - S \propto -\sum_f P(f_a) \ln [P(f_a)/P^o(f_a)]. \tag{7}$$

If some unspecified external constraints act on the particles which prevent the prior distribution from being realized, the most probable distribution will be the one that minimizes the entropy difference ΔS. This will occur when the ratio of the two functions $P(f)/P^o(f)$ is a maximum. The function $P(f_a)$ can thus be obtained with the aid of Lagrange maximization which leads to a simple exponential function, i.e.

$$\ln [P(f_a)/P^o(f_a)] = \lambda_0 + \lambda_1 f_a + \lambda_2 f_a^2 + \ldots + \lambda_1 f_a^i + \ldots. \tag{8}$$

The λ-parameters thus introduced reflect the constraints that act on the reagents during the interaction that distort the distribution from the 'prior' equilibrium form. They can be expressed as

$$\lambda_i = \frac{\partial \Delta S}{\partial \langle f_a^i \rangle}, \tag{9}$$

where $\langle\ \rangle$ indicates the average value of f_a^i. If all of these averages are equal to those given by the prior distribution (i.e. they correspond to those for a gas in equilibrium), the λ_i-parameters will be zero.

With the addition of the maximum entropy term the probability density function for the fraction of energy in mode a now takes the form

$$P(f_a) = \frac{\Gamma(\Xi_a+\Xi_b)}{\Gamma(\Xi_a)\,\Gamma(\Xi_b)}(f_a)^{\Xi_a-1}(1-f_a)^{\Xi_b-1}\exp(-\lambda_o-\lambda_1 f_a-\ldots). \tag{10}$$

The above analysis for the derivation of the final distribution is valid regardless of the selection of the prior distribution, provided that the latter in some sense maximizes the entropy of the system. The present analysis shows that the existence of non-zero λ-parameters indicates a departure of the final distribution from the prior distribution. The problem that remains is the derivation of the λ-parameters.

3.3. *Derivation of the λ-parameters*

The first constraint that applies to all distributions is the condition of normalization, i.e. the total probability is unity

$$\int_0^1 P(f_a)\,\mathrm{d}f_a = 1. \tag{11}$$

This condition cannot be used to discriminate between the prior and the actual distribution since it applies to both. Higher-order constraints are associated with expressions for moments of $P(f_a)$, namely

$$\int_0^1 f_a^n\,P(f_a)\,\mathrm{d}f_a = \langle f_a^n\rangle. \tag{12}$$

Successive application of this equation permits the remainder of the λ-parameters to be determined. For $n = 1$, equation (12) ensures that all possible distributions have the same average energy.

For a practical application of the method, the aim will be to determine the probability distributions with sufficient precision by using the minimum number of constraints since, in general, the moments of the actual distribution are unknown. Comparison between the distributions obtained using this analysis and experimental measurements have been made for many reactions including those involving air species. Remarkably, the experimental evidence (Levine & Bernstein 1987) shows that in most cases only the first two terms, λ_0 and λ_1, are needed to describe the deviation of the final distributions from the prior ones with acceptable precision. The distribution therefore can be simplified to

$$P(f_a) = \frac{\Gamma(\Xi_a+\Xi_b)}{\Gamma(\Xi_a)\,\Gamma(\Xi_b)}(f_a)^{\Xi_a-1}(1-f_a)^{\Xi_b-1}\exp(-\lambda_0-\lambda_1 f_a). \tag{13}$$

Higher-order terms can be added if judged necessary for certain reactions. The λ_0 factor can be evaluated without the use of experimental data. However, for the DSMC computations, a select–reject scheme is used to obtain the required random samples of the post-collision energy levels from the distribution $P(f_a)$. To do this, the distribution is first normalized and thus the constant terms (the Γ-function terms and the factor $\exp(-\lambda_0)$) do not have to be calculated and only λ_1 is needed. In the following analysis

we will assume that λ_0 and λ_1 suffice to describe the distributions and, as only the latter has to be evaluated, it will henceforth simply be referred to as λ.

4. Theory of chemical reactions

The activation energy has traditionally been used as a measure of the energy required to initiate a chemical reaction when the reagents are in thermodynamic equilibrium. This criterion fails when the reagents are not in equilibrium. In these circumstances it is necessary to quantify the importance of each energy mode separately in promoting the reaction.

There has been considerable debate regarding the role of the different energy modes in promoting reactions. In principle all those present can contribute to overcoming the energy barrier, but experiments confirm that not all modes are equally efficient in promoting a reaction. For example, in the case of dissociation, the energy contributed by the vibrational modes is recognized as being the most effective agent promoting the reaction. All of the other modes (rotational, electronic, translational) can in some circumstances contribute to the chemical activity, either explicitly (excitation of the electronic mode is mainly responsible for the ionization of a particle) or implicitly, since exchange of energy is possible between the available modes during the course of a collision – a process that becomes increasingly more important in high-energy collision when exchange between the various modes during an interaction is relatively easy. This gives rise to the appearance that all energy modes are equally effective in promoting the reaction.

A second important characteristic of chemical reactions is the link between the specificity in the post-collision energy redistribution for a forward reaction and the selectivity in the energy consumption of the corresponding reverse reaction. An example of particular importance in atmospheric chemistry is the case of the recombination reactions, of the form $A+B+M \rightarrow AB+M$. These are observed to produce vibrationally highly excited products. Their reverse dissociation reactions take place preferentially from reagents that are in highly excited vibrational states. In short, if a forward reaction favours some energy states of a particular energy mode, then the reverse reaction will proceed with greater efficiency if the energy is in that state rather than in any other mode. The phenomenon is a manifestation of the principle of *microscopic reversibility*. Simply stated: *the probability of an energy state causing a reaction should equal the probability of this energy state being populated after the reverse reaction.*

4.1. *Chemical reaction model*

The implication of the principle of microscopic reversibility is that exactly the same formula that has been used for the energy disposal (equation (13)) can be used for the prediction of the probability of the corresponding reverse chemical reaction. The prior distribution represents the most probable incident energy distribution for a collision to lead to a reaction at a given total energy without a preference towards any energy state. However, for the real reactions, and within the ME formulation, it is again the λ-parameters that embody the 'constraints' imposed on this distribution changing it from the equilibrium one to the real distribution. Consistent with the micro-reversibility argument and since the prior distributions for energy exchange and chemical reactions are identical, *the λ evaluated for the reaction probability will be exactly the same as those for the energy disposal of the corresponding reverse reaction.* The correspondence of the λ-parameters and prior distributions for energy exchange and reaction means that the method automatically satisfies detailed balance (see Levine

& Bernstein 1987), which is the outcome of achieving micro-reversibility with equation (13).

Adopting a general approach to the problem, it can be stated that all available energy modes can potentially contribute to promoting a reaction. The reaction probability P_r at a total energy E can thus be expressed as

$$P_r(E) = S_f P(E_{vib}, E_{rot}, E_{trans}, E_{elec}), \tag{14}$$

where if i represents the vibrational, rotational, translational and electronic modes (designated as *vib*, *rot*, *trans* and *elec* respectively), $P(E_i, \ldots)$ is the probability of energy E_i in mode i causing a reaction, and S_f is a steric factor that takes into consideration the orientation of the colliding particles. For most of the reactions of interest in atmospheric re-entry chemistry it is possible to identify one energy term from equation (14) that dominates the reaction while the others appear to have little influence. Hence to simplify the calculation of the probability we will assume that the reaction is controlled by one mode only, i.e. $P_r(E) = S_f P(E_i)$ and the probability $P(E_i)$ will be obtained from equation (13). However, it should be emphasized that this assumption is not a necessary condition for the application of the method.

Estimates of the λ-parameter are required for each reaction over a range of energies. In the experimental studies made by Levine & Bernstein these parameters were found to be functions of the total interaction energy, E. In line with the observations that all the energy modes become equally effective in promoting the reaction at very high collision energies, the energy distributions should tend towards the equilibrium ones (i.e. the λ should tend to zero) as the collision energy increases. In earlier work (see Gallis & Harvey 1993) λ was arbitrarily modelled as a simple linear function of the reaction energy tending to zero for the highest energies likely to be experienced, i.e.

$$\lambda = \lambda_c + \lambda_T E_{trans}, \tag{15}$$

where λ_c and λ_T are constant parameters, which are estimated by comparing the ME reaction rates predicted by single-cell numerical simulations with available experimental data (see §5.2).

The chemical reactions of interest in rarefied hypersonic aerodynamics can be divided into two main types in terms of their energy dependence. These are the dissociation reactions and the exchange reactions. These will be examined separately.

4.2. *Dissociation reactions*

Dissociation reactions are the first to take place in re-entry flows and are of the form

$$AB + M \rightarrow A + B + M, \tag{16}$$

where AB can be O_2, N_2, NO or the corresponding ions, O_2^+ etc. Correct modelling of these reactions is important not only because they initiate the chemical processes but also because they have a large endothermicity, i.e. they absorb considerable energy from the flow.

It is generally perceived that the vibrational excitation of polyatomic particles plays a decisive role in initiating dissociation. To calculate the reaction probability for dissociation equation (13) can be applied where the mode i is the vibrational mode. The influence of the vibrational energy on the reaction probability is also dependent on the total energy available in the collision. The enhancement of the endothermic reaction rates by the vibrational energy has been found (Levine & Bernstein 1987) to be high for low energies but as the energy of the reaction increases its influence diminishes. This

phenomenon, which has been neglected in other DSMC chemistry models, can be modelled with the ME method by the use of a λ-parameter that is a decreasing function of the collision energy as suggested in equation (15).

To calculate the energy disposal after the chemical reaction, the λ used for the reaction probability of the reverse reaction is required. In our implementation of the method, where only one energy mode is assumed to control the reaction probability directly, the distribution of this energy mode only can be influenced by the λ-parameter; the energy in the other modes will thus be distributed according to the equilibrium distributions (i.e. $\lambda = 0$ is assumed for the other modes).

For exothermic reactions (e.g. recombination reactions), the increase in the rate as a result of added reagent vibrational energy is lower than expected from the equilibrium distributions, i.e. vibrational energy discourages these reactions from taking place. This is in direct contrast to endothermic reactions. The recombination reactions require three-body collisions and they will not be treated in this study since in rarefied flows they only rarely occur. They can, however, be modelled using the same principles as the dissociation reactions.

4.3. *Exchange reactions*

The second group of reactions in atmospheric chemistry is the *atom exchange* or *shuffle* reaction type. These can generally be described as

$$A + BC \rightarrow AB + C \tag{17}$$

and they are very significant since 30 out of the 65 most common ones fall within this category. They have a smaller energy threshold than the dissociation reactions and hence they take place more often once the appropriate species, which cascade down from the dissociation reactions, are present within the flow. Owing to their smaller energy threshold they have less effect on the total energy of the flow than the dissociation type but they play an important role in the balancing of the chemical species and energy modes. It follows that correct modelling of these reactions is essential because of their controlling influence on the flow.

Unlike the dissociation reactions, most of the exchange reactions appear to be insensitive to the amount of energy in the vibrational mode but the reaction cross-sections depend principally on their translational energy. An important group of reactions in atmospheric chemistry that present such a behaviour are the exothermic-ion–molecule exchange reactions:

$$N^+ + O_2 \rightarrow \begin{cases} NO^+ + O \\ N + O_2^+ \end{cases}. \tag{18}$$

The ME formulation of the reaction probability for these reactions follows the same pattern as for the dissociation reactions but with a dependence on the translational energy replacing one depending on the vibrational energy. Equation (13) is perfectly symmetric for all energy modes and the term Ξ_a can simply be replaced with the translational degrees of freedom. In the absence of better information, again a linear dependence of the λ-parameter on total energy has been selected. The energy exchange for the exchange reactions is formulated to satisfy the principle of microscopic reversibility.

The Appendix contains a list of the reactions that have been incorporated into the DSMC code with their corresponding controlling energy mode. The reactions involving ionized species have been excluded from the flow field examples presented in the present study but are listed in the Appendix for completeness.

4.4. *Implementation of the ME method*

The use of the Borgnakke & Larsen model for the prior distribution offers a computational advantage within the DSMC code, as both the reacting and non-reacting collisions can be dealt with in a single routine. For the latter, the λ-parameters are set to zero and the ME model reduces to a conventional Borgnakke & Larsen internal–translational energy exchange as proposed by Bird. In this study the vibrational mode is treated as a quantized energy distribution complying with the harmonic oscillator model. The so called *generalized Borgnakke & Larsen method* (see Bird 1994) which is a quantized serial application of the method has been used. It should, however, be noted that the ME model can be used for either continuous or quantized distributions of energy. For the energy exchange after chemical reactions that are sensitive to the vibrational energy, the exponential term is added to the vibrational energy distribution to account for the effects of non-equilibrium. The rotational and the translational energy modes are treated as continuous energy distributions. The parameters used for the energy exchange are the same as those chosen for the calculation of the reaction probability of the corresponding reverse reactions. This ensures micro-reversibility.

5. Results

5.1. *Blunted-cone flow without chemistry*

Before presenting examples of calculations involving chemistry, results for a non-reacting flow will be given to illustrate the use of the DSMC code. The rarefied hypersonic flow around at 70° spherically blunted sting-mounted cone will be studied and compared with measured data. This shape has attracted considerable attention as it is a serious contender for an aerobrake Earth return module of an envisaged NASA Martian Explorer spacecraft. It has also been chosen by the AGARD Working Group 18 as a test case and, as a result, a number of high-quality measurements have been obtained for this geometry under rarefied conditions. Unfortunately, as yet, the experiments have been restricted to enthalpies too low for reactions to take place within the flow.

The conditions of the numerical simulation are the same as those of an experiment conducted by Allegre & Bisch (1996*a*, *b*) in the SR3 tunnel at CNRS in Paris. In this, measurements of the heat transfer to the surface of the body and sting and flow field density were made. The latter were obtained using electron beam fluorescence. The base radius R_b of this body was 25 mm and the radius of the nose was 12.5 mm. The cone was supported by a sting of 6.25 mm radius (see figure 1). The conditions of this experiment are given in table 1.

The DSMC simulation was performed using a refined computational grid of 12000 cells and 500000 particle simulators. Most of the cells (around 10000) were gathered in front of the body where the higher densities are found. 25000 time steps were executed and steady-state sampling started after 15000 time steps.

The density profile for the flow field is given in figure 1; non-dimensionalization has been done with respect to the free-stream density.† In this figure the flow comes from left to right. In front of the body a diffuse shock wave forms, behind which subsonic

† For convenience, henceforth this non-dimensional quantity will be referred to simply as the density and in common with all other plots presented in this paper, the curves are drawn directly from the raw computer results. No smoothing has been applied, which accounts for the slight unevenness of some of the contours.

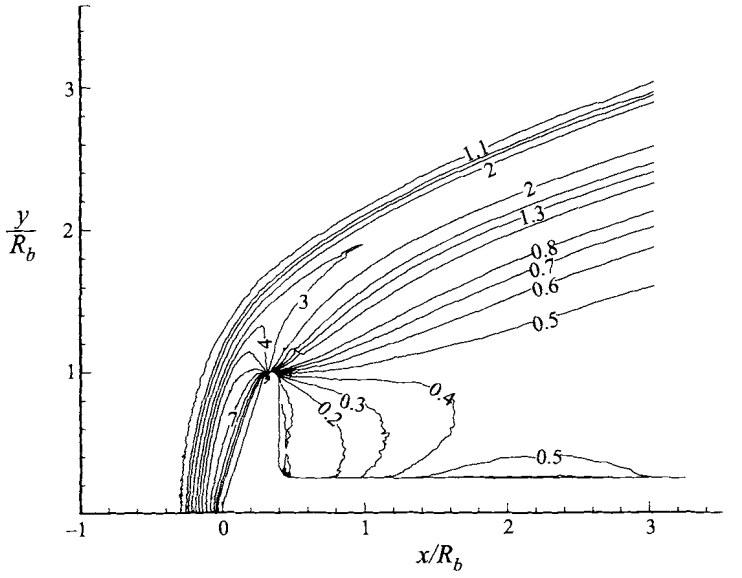

FIGURE 1. 70° Cone, SR3 case. Numerical prediction of the flow field density.

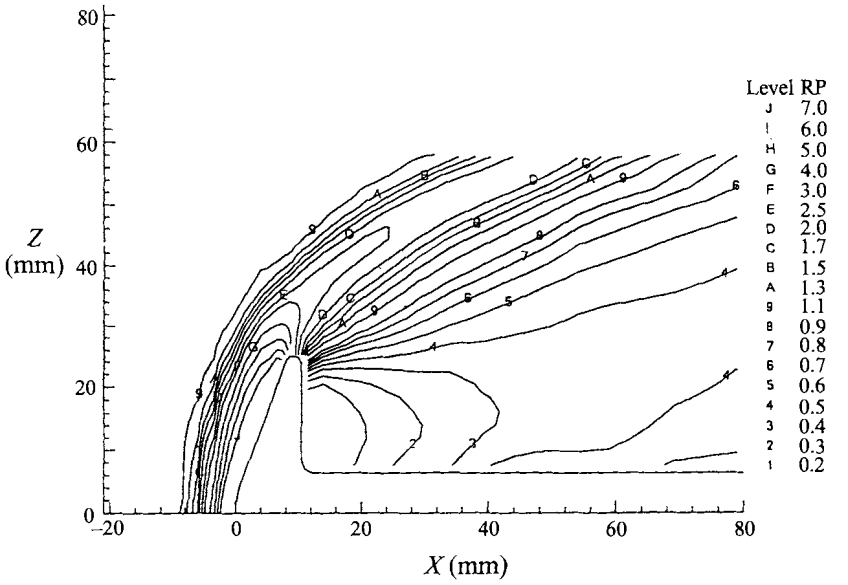

FIGURE 2. 70°: Cone, SR3. Experimental measurements of the flow field density taken from Allegre & Bisch (1996*a*).

Mach number	20
Stagnation temperature (K)	1100
Stagnation pressure (bar)	10
Reynolds number (cm^{-1})	838

TABLE 1. Conditions of the SR3 test

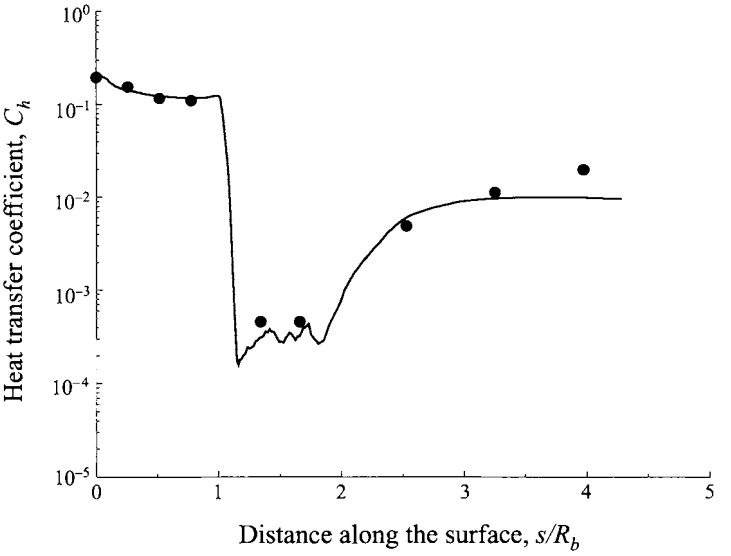

FIGURE 3. 70° Cone, SR3 case. Numerical prediction for the heat transfer coefficient (——) compared with experimental measurements (●).

flow extends from the axis to very close to the outer rim of the body. Downstream of the body and between $x/R_b = 0.4$ and 1.6, a low-density re-circulating wake area is formed. A very diffuse oblique recompression shock originates at about $x/R_b = 2$ which is associated with the flow reattachment on the sting. The density peaks to around 50% of the free-stream density in this recompression. Allegre & Bisch (1996*a*) measured electron-beam density profiles are reproduced in figure 2. These results have been corrected by Allegre, by a few percent, to compensate for slight flow non-uniformity measured in the empty wind tunnel. The measured and calculated results can be seen to be in excellent agreement, both in the low-density area behind the body and in the higher density associated with the shock wave. The most notable difference is a small discrepancy between the results in front of the body for densities in the range 1.05 to 2.0.

The calculated heat transfer distribution to the surface of the vehicle is presented in figure 3. The heat transfer coefficient has been defined as

$$C_h = \frac{\dot{q}}{\frac{1}{2}\rho u^3}, \tag{19}$$

where $\dot{q}$ is the heat flux per unit surface area and ρ and u the free-stream density and velocity respectively. The horizontal axis is based on the distance s measured along the surface of the body from the stagnation point. Allegre & Bisch's measured values are also shown as symbols. As expected the maximum value of the heat transfer is found at the stagnation point. From here, after a relatively flat area that corresponds to the forebody, the heat transfer exhibit a slight local peak at the shoulder of the cone and then drops by 3 orders of magnitude on the back of the body to a level that proved difficult to measure. This drop in the heat transfer is due to the rapid expansion around the outer rim of the body. The experimental results shown for the base of the cone in the range $s/R_b = 1.1$ to 2.0 are, according to Allegre & Bisch, the upper bound of possible measured values. The heat transfer starts to rise again along the sting towards the reattachment point at about $s/R_b = 2$ and finally in the stimulation reaches a

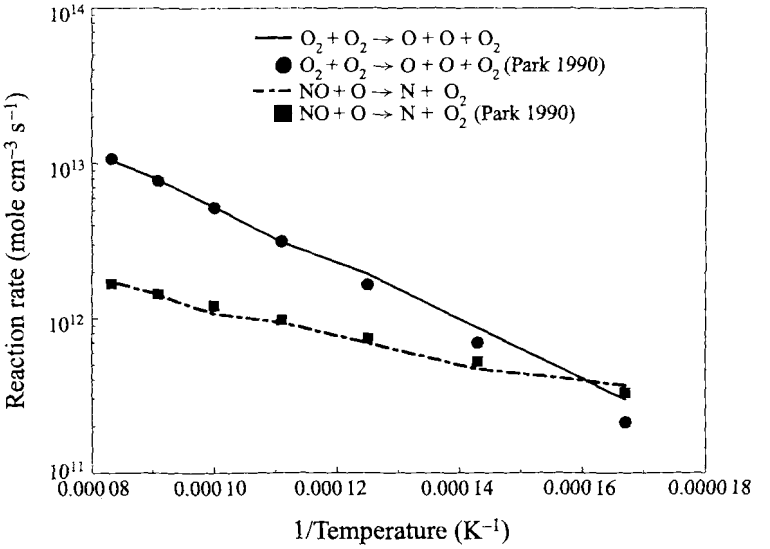

FIGURE 4. Maximum Entropy simulation of chemical reaction rates at equilibrium.

plateau. Good agreement is achieved with all of measurements except for the most downstream point on the sting which is higher than the rest of those in the plateau. This discrepancy can be explained by the forward interference effect of a larger diameter downstream sting support which was not modelled in the simulation.

5.2. *Single-cell reaction rate simulation*

The first requirement of a chemical reaction model is that it is able to reproduce the correct Arrhenius reaction rates for a near-equilibrium gas over a representative range of temperatures. There is a considerable volume of experimental data for these rates for most of the reactions of interest in hypersonic aerodynamics but, because of the high temperatures at which they occur, the measurements are generally in poor agreement with each other. Deciding which are the most accurate results is a difficult task but, fortunately, Park (1990) has made an extensive critical evaluation of all of the experimental evidence for a wide variety of reactions. His compendium of recommended rates is generally considered to be the most reliable. Unfortunately, his published data are limited to temperatures from 3000 to 10000 K which correspond only to the lower end of the span of interest for re-entry flows.

The reaction rates at equilibrium achieved by a molecular model can be tested by performing a single-cell DSMC simulation. One way of doing this is to use an ensemble of particles to represent the reacting species which are assigned initial energies according to the equilibrium distributions at a specified temperature. Within this simulation, particle pairs are chosen at random at a fixed rate and each collision is examined to ascertain whether the model being tested would have indicated that a reaction would have occurred. Successful events are recorded as reacting collisions, although the energy and species of the colliding partners are left unchanged in order to retain the initial composition and equilibrium state of the gas mixture. The reaction rate at equilibrium is thus deduced from the frequency of encounters that lead to reactions. The simulation can be repeated for different temperatures and, hopefully, by adjusting the parameters in the collision model, a satisfactory match with the experimental data can be achieved over the desired range of temperatures.

Figure 4 shows a sample of the reaction rates obtained with the present ME model

from a single-cell simulation over a range of temperatures for representative dissociation and exchange reactions, namely

$$\left.\begin{aligned} O_2+O_2 &\rightarrow O_2+O+O, \\ N_2+0 &\rightarrow NO+N. \end{aligned}\right\} \tag{20}$$

The rates that have been achieved are compared with Park's suggested values for the same range of temperatures. The linear temperature dependence of λ described in equation (15) and individual constant parameters have been used for each reaction. The figure shows that it is possible to obtain good agreement with the measured reaction rates despite the small number of parameters that can be adjusted. Park estimates that his rates could possibly be in error by a factor of 2 to 3 and all of the simulated results are well within this range. The match has been achieved with relative ease and although it is also possible to do this with the original Levine & Bernstein formulation, it is generally a more difficult task and the agreement over the full temperature range is inferior.

The non-equilibrium aspects of the collision model cannot be verified for the air reactions as there are no suitable measured data available. Such information could, in principle, be obtained experimentally, for example by using crossed molecular beams but so far this has not been attempted for any of the reactions of interest at the appropriate energy levels. For most of the reactions there is general consensus as to which is controlled by either the vibrational or translational energy and this information has been used to construct the models.

Unfortunately there is also a dearth of reliable experimental results for reacting rarefied hypersonic flow fields which could be used for the indirect validation of a chemistry model. Although a few contemporary wind tunnels are able to reproduce these flows, the instrumentation has not yet been developed to a stage where precise measurements of species concentration or energy states within specific modes can be made with sufficient precision for validation purposes. Flight data cannot be used with confidence as these are subject to larger experimental errors than achieved in the ground-based facilities. Interesting conclusions can however be made by comparing the predictions made with the present model and other methods.

5.3. *Shuttle Orbiter simulation*

The first flow example to be considered in which chemical reactions take place is the flow around the nose region of the Shuttle Orbiter. Results have previously been published by Carlson & Bird (1995) using Bird's chemistry and energy exchange models. They used an axi-symmetric DSMC code (see Bird 1994) to obtain data along the stagnation streamline of this vehicle when flying at 92.35 km altitude. The nose area of the shuttle was simulated by a hyperboloid of nose radius $R_N = 1.296$ m and asymptotic half-angle 41.15°. The surface temperature of the vehicle was assumed to be 1043 K. In our study the flow field predictions have been made with a DSMC code employing our ME method. The ambient air conditions were taken from the US Standard Atmosphere Tables (1976) for 92.35 km altitude but the fluid was a pure N_2–O_2 mixture (0.783:0.217 mole fraction ratio). In both cases the body was assumed to be moving at a velocity of 7.5 km s^{-1} at zero angle of incidence. In this and in subsequent examples the effect of ionizing reactions has been ignored.

A contour plot showing the flow field has not been presented for this example as in many respects it is similar to that for the blunter cone shown in figure 1. The forward face of the cone is enveloped with a diffuse shock wave and, between this and the body, a very hot shock layer is formed in which a complex series of chemical reactions takes

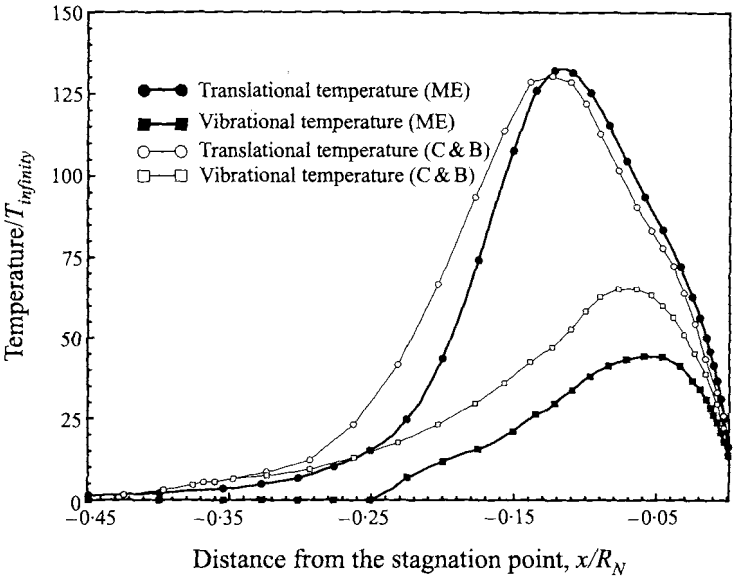

FIGURE 5. Comparison of temperature profile along the stagnation streamline for the Shuttle Orbiter at 92 km altitude between the Maximum Entropy method and Carlson & Bird's (1995) simulation.

place due to the compression heating. The translational and the vibrational temperature profiles along the stagnation streamline are presented in figure 5, normalized with respect to the free-stream temperature which was 180 K. These profiles given an indication of the physical processes taking place within the flow ahead of the body. In this figure the flow is from left to right and the stagnation point is at $x/R_N = 0$. The translational temperature rises to a maximum of about 130 times the free-stream temperature followed by a peak in the vibrational temperature. These temperatures are high enough to provoke chemical reactions within the flow. The vibrational temperature has a maximum value of around 45 times the free-stream temperature in the shock layer where the flow is chemically active.

The results of the Carlson & Bird simulation are also presented in the same figure as open symbols. The levels of translational temperature in their calculation are similar to ours but they rise to a slightly lower peak value. The striking difference is in the vibrational temperature which is about 3500 K higher in the Carlson–Bird calculation. It can be seen that nowhere in the flow (apart from at the surface of the body) is thermal equilibrium achieved in either calculation. The initial rise in vibrational temperature is very different in the two calculations. For the ME model this component remains unexcited until about $x/R_N = -0.23$ where there is a small but sharp rise followed by a more gradual increase. With the Bird model this component rises earlier and more smoothly. The behaviour of the vibrational temperature on the upstream side of the shock wave is sensitive to, and closely linked to, the initiation of chemical reactions, in this case the onset of the dissociation of oxygen followed later by nitrogen. It is also sensitive to the internal energy exchange modelling which, for non-reacting collisions in these simulations, is computed for each particle individually using variable vibrational and rotational exchange restriction factor numbers. Although the position where the translational temperature first begins to increase is about the same in both simulations (at $x/R_N \simeq -0.40$), the point where this accelerates to a rapid rise (which coincides with the place where the first detectable density increase takes place) is closer

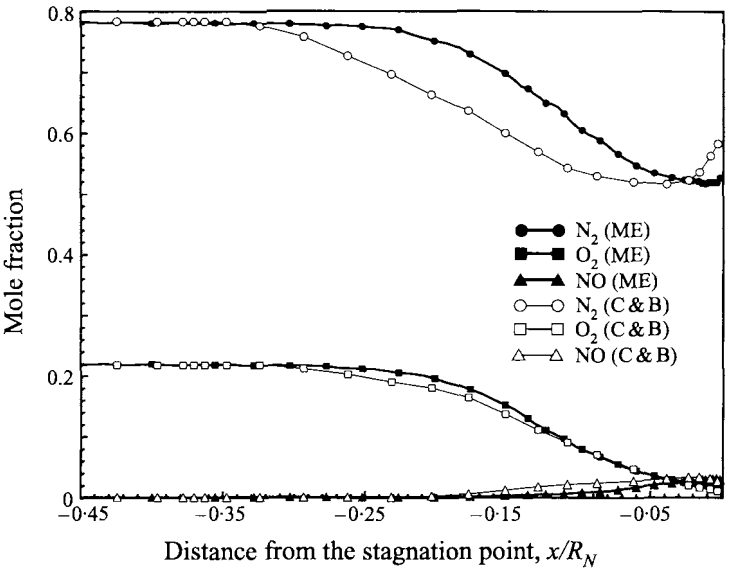

FIGURE 6. Comparison of species mole fractions along the stagnation streamline for the Shuttle Orbiter at 92 km between the Maximum Entropy method and Carlson & Bird's (1995) simulation.

to the surface (at about $x/R_N = -0.23$) for the ME model. The shock layer is thus thinner.

The differences in the vibrational temperatures in the two calculations reflect changes in the predicted chemical activity. A comparison of the chemical synthesis is presented in figure 6. For the ME calculation dissociation of N_2 starts at about the same vibrational temperature as the Bird prediction but proceeds more slowly owing to the lower vibrational temperature. For the ME model, N_2 dissociation commences at about $x/R_N = -0.23$ and this is linked to the sudden jump in the vibrational temperature seen in figure 5. Deeper within the shock layer the level of N_2 concentration falls to the same minimum for both methods, presumably because the flow is approaching near equilibrium by this point. This illustrates that both codes behave in a similar manner for near-equilibrium situations.

Oxygen, having a smaller energy threshold, is less affected by the differences in the temperatures and, once the translational temperature has exceeded the dissociation threshold and there are sufficient collisions (i.e. the density has risen sufficiently), dissociation takes place. It should be remembered that although the vibrational energy is used to control the dissociation reactions, the first criterion for a reaction to take place is that the collision energy exceeds a specific threshold. The two models have similar dependence on the vibrational energy for dissociation reactions but it can be seen that there is some measurable divergence in the region of greatest non-equilibrium.

The production of nitric oxide, NO, in these flows is an important factor as it is used for the remote optical sensing of re-entry vehicles. This process is strongly influenced by the differences in the temperatures in the two simulations. Bird's method predicts a higher mole fraction of NO than the ME method by a factor of more than 2. This result is to be expected since Bird's method results in an overall more chemically active flow due to the higher vibrational temperatures.

The prediction of lower vibrational temperatures by the ME model is attributable to both the different energy exchange process and different chemical reaction model. This

flow field example is dominated by dissociation reactions and for these the ME scheme (*a*) favours the depletion of the high vibrational energy states after the dissociation reactions and (*b*) yields reaction products that are vibrationally cooler in order to satisfy detailed balance. These differences between the two models become increasingly prominent for flows that are more rarefied and/or chemically active.

5.4. *A 70° spherically blunted cone at 85 km*

In the second reacting-flow example the 70° spherically blunted cone that has already been investigated in §5.1 will be reconsidered but under conditions that correspond to hypersonic flight in a nitrogen–oxygen gas at the density and temperature found at an altitude of 85 km in the Earth's atmosphere. The simulation has been conducted for the vehicle of base radius 1 m, flying at a velocity of 7.5 km s^{-1} at zero angle of incidence. The velocity is sufficient to promote more intense chemical reactions than in the previous example but not energetic enough to cause significant ionization. At this altitude considerable rarefaction and non-equilibrium effects will be experienced and the heat transfer, while not at its maximum, will nevertheless be very appreciable. Most of the interesting chemical activity occurs ahead of the upstream face of the body and thus to reduce the computing time only the flow field up to the outer rim has been simulated. As this flow bears a number of similarities to the first reacting example a discussion of the results will be brief.

For comparison, a supplementary computation has been made for this body under exactly the same conditions but with all of the reactions inhibited. This solution is obviously unrealistic, but it serves to highlight the effects of chemistry on the flow.

Figure 7(*a*) shows contours of the density for the two computations: the contours from the one with full chemistry are shown in the upper half of the illustration mirrored against those without chemistry in the lower half. The flow is from left to right.

For the non-reacting flow the presence of a diffuse shock can be clearly identified, in which the density rises ahead of the body from the free-stream value to about 7 – a little above the Rankine–Hugoniot value for a perfect gas. Behind this shock there is a plateau extending to close to the body surface where the density rises sharply owing to cooling by the wall. Note that irregular intervals between contours have been chosen from this region for clarity. The separation between the shock and the body surface increases radially outwards from the axis. In figure 7(*b*) the corresponding Mach number contours for this flow are plotted. The shock layer (i.e. the region between the shock wave and the fore body surface) is, as expected for this cone angle, an area of subsonic flow, terminated by a sonic line located close to the rim of the body. This line, which lies more or less normal to the radial outflow, marks the beginning of the rapid expansion around the rim of the body and it explains the closely spaced group of contours in figure 7(*a*) around $y/R_b = -1.0$, close to the surface where a very sudden fall in density in the radial outflow behind the shock is witnessed. Associated with this is a sudden drop in the temperature which would have effectively frozen all of the chemical reactions had they been permitted. The increase in velocity near the rim causes a small localized peak in the heat transfer.

Quite significant differences are seen between this flow and the reacting one depicted in the upper half of figure 7(*a*). It is immediately evident that the shock stand-off distance is roughly halved and there are marked changes in the contour patterns. The effect of the predominantly endothermic dissociation reactions is to reduce the flow temperature; this in turn increases the density which leads to a thinning of the shock layer in order to maintain continuity in the radial outflow mass flux. Despite the

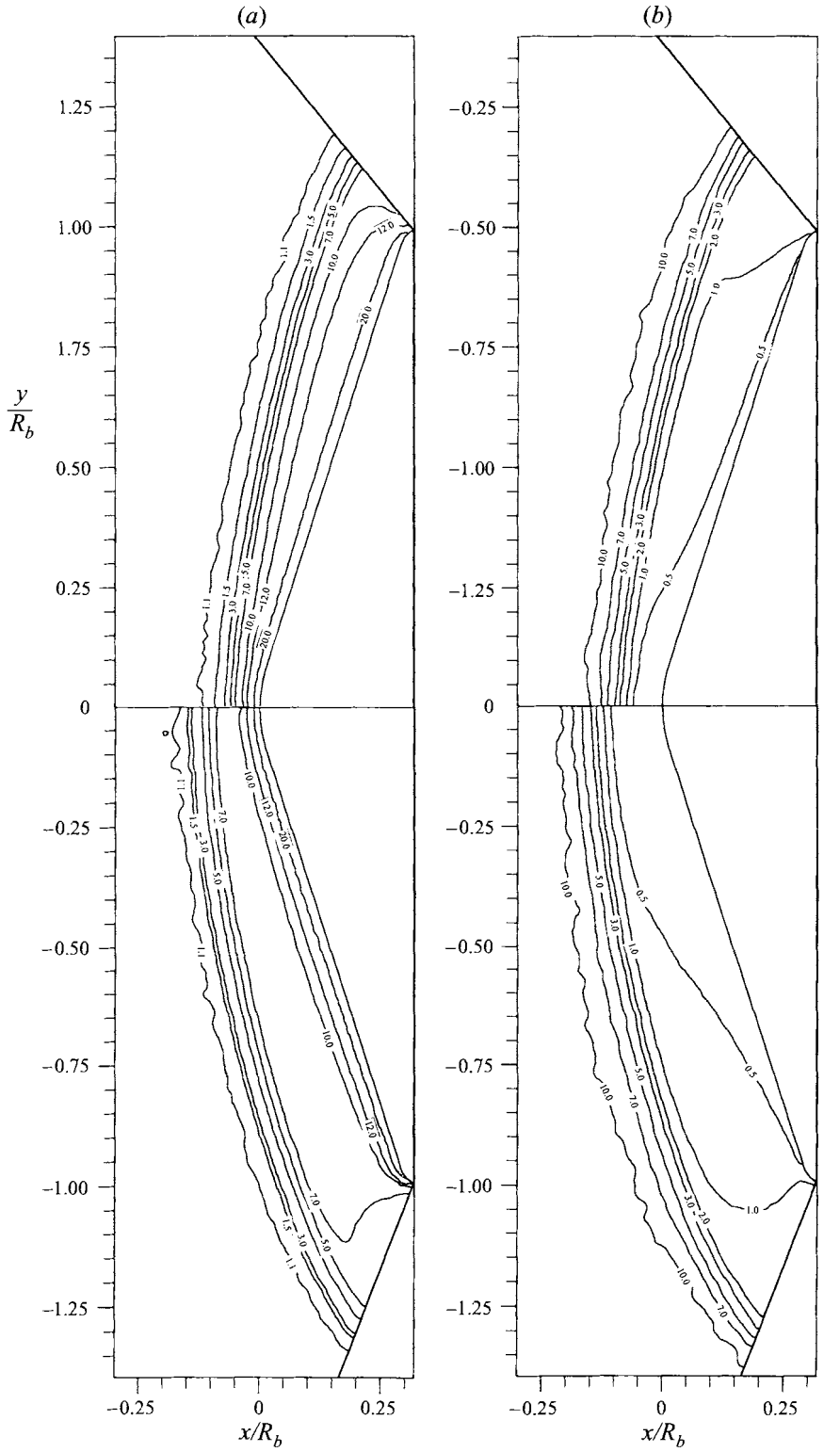

FIGURE 7. (*a*) Density prediction and (*b*) Mach number contour lines for the flow field of the 70° cone. Upper half: reacting case; lower half: non-reacting simulation.

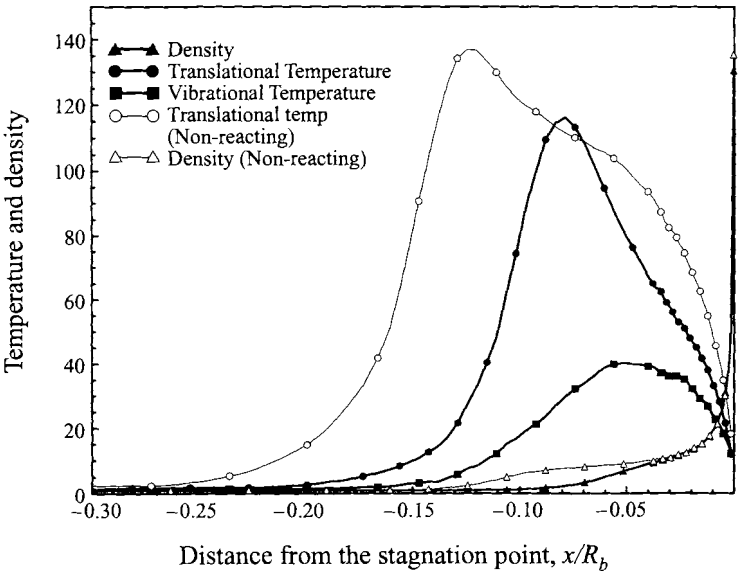

FIGURE 8. Density and temperature profiles along the stagnation streamline for the 70° cone.

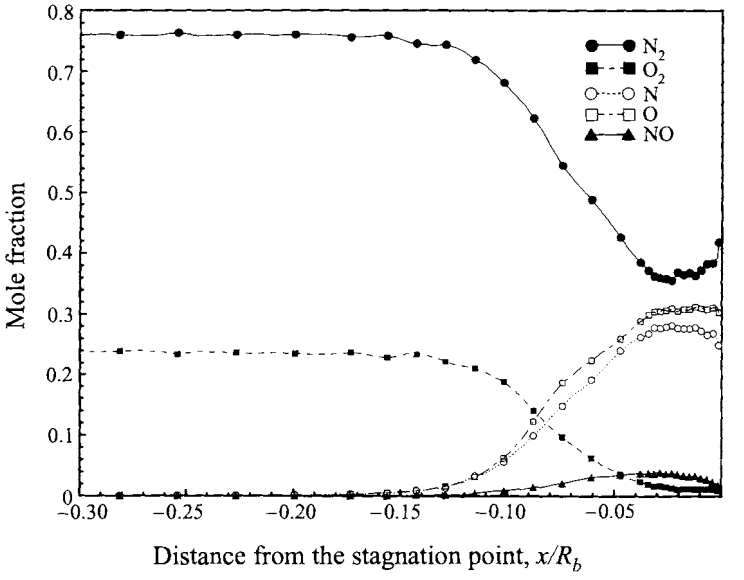

FIGURE 9. Species mole fraction along the stagnation streamline for the 70° cone.

chemical activity within the flow, these simultaneous changes leave the pressure acting on the forebody, and hence the drag, almost unchanged. The Mach number contours shown in upper half of figure 7(*b*) reveal that the flow within the shock layer has a generally higher subsonic value when the reactions take place. This is due primarily to a reduction in the sound speed caused by the lower temperature. The sonic line moves nearer the flow axis and lies obliquely to the radial outflow.

As in the previous example, the quantitative effects of the chemistry can be seen clearly from profiles plotted along the stagnation streamline. Profiles of density and temperature are presented in figure 8 and of species mole fractions in figure 9. The flow is approaching from the left and the stagnation point is at $x/R_b = 0$. In the first of these

figures the density profile confirms the observation made about the shock when discussing figure 7(*a*). For the reacting flow it can be seen that the diffuse shock wave, which forms at about $x/R_b = -0.06$, is followed immediately by a further rise due to the influence of the cold wall and the shock and boundary layer are 'merged'. The shock does not conform to the Rankine–Hugoniot structure. The expected reduction in the temperature due to the reactions is clear from figure 9.

Figure 10 shows that the mole fraction of N_2 reduces from about 0.8 to 0.35 in passing through the shock layer. This confirms that the temperatures are high enough to provoke dissociation and, as the flow is more energetic than in the Shuttle Orbiter example, this is more complete. N_2 and O_2 dissociation starts simultaneously with the rise in vibration temperature at about $x/R_b = -0.15$, indicative of the coupling between these processes. By about $x/R_b = -0.03$ the O_2 dissociation is almost total, owing to its lower energy threshold than that for N_2.

The production of NO in this flow is greater than in the example of the Shuttle Orbiter given in §5.3. It begins to appear shortly after the onset of dissociation of the diatomic species which is earlier than in the previous example. The mole fraction reaches a local maximum at about $x/R_b = -0.03$. As the density rises near the surface, NO dissociates in the same way as the other molecular species.

The dissociation of the molecular species is followed by the appearance of atomic species which were not present in the simulated free-stream flow, although some O would have been found in the real atmosphere at these altitudes. It is interesting to note the localized change in the mole fraction of the atomic species near the surface. The fraction of atomic nitrogen drops while that for atomic oxygen increases. Since the recombination reactions were not included in this study, these changes are due to the low energy threshold exchange reactions that take place in this area. It is thought that this behaviour must be primarily attributable to the reaction $NO + N \rightarrow N_2 + O$ and secondly to $O_2 + N \rightarrow NO + O$. Although there are no experimental data to validate this proposition, they are the only O-producing and N-depleting reactions that can take place in this area.

The conditions of this and the previously simulated case correspond to flight conditions that could be met during re-entry. It is worth noting that, apart from the area close to the body where the densities are very high, nowhere is thermodynamic equilibrium attained. This observation justifies the initial requirement that any chemical reaction and energy exchange model used should incorporate the effects of thermodynamic non-equilibrium. The unavailability of precise experimental flight data makes it impossible, for the time being, to validate any of the available chemistry models. The only possible comparisons that can be made at present are with the results of other Navier–Stokes and DSMC codes. As these universally use as their basis the equilibrium Arrhenius reaction rates and, if they are molecular simulations, the Borgnakke–Larsen distributions, they are built on the implicit assumption of local molecular equilibrium which has been avoided in the present work. This raises the inevitable question of to what extent this difference influences the final results. The answer depends on what is being sought from the computations and within which regime the flow takes place. The influence of non-equilibrium depends on the degree of rarefaction and on the reactivity of the flow. The examples cited above for high-altitude flows show that changing the reaction model alters the distributions of energy within the flow. This, in turn, influences the mole fractions of some species. The level of nitric oxide, for example, can be doubled and, as this a crucial component of the flow in signature-recognition applications, the effect is very important in some instances. Likewise the levels of heat transfer to the body surface are influenced by the chemical

activity. Precise evaluation of the heating of a re-entry body will rely on accurate simulation of the real gas effects including the non-equilibrium phenomena. On the other hand the pressure and drag are almost totally unaffected.

6. Conclusions

The non-equilibrium chemical reactions and energy exchange that take place in hypersonic flow fields have been examined within the framework of the DSMC methodology. The generalized Borgnakke & Larsen (1975) model has been extended to include the effects of non-equilibrium energy exchange following chemical reactions. This extension has been done with the aid of the Maximum Entropy method, originally developed by Levin & Bernstein (1987), but modified here to include the effects of the molecular model in the energy exchange distributions. This has ensured realistic modelling of the transport properties of the fluid. Using the principle of microscopic reversibility the reaction probability is linked to the energy disposal of the reverse reaction. This allows the same techniques that have been used for the prediction of the post-collision energy disposal to be used to predict the probability of chemical reactions taking place. The present implementation of the ME method for the prediction of chemical reactions takes into consideration the energy mode that is particularly effective in promoting a reaction once the collision energy threshold is exceeded and scales it according to the total energy. The dependence of the method on the principle of microscopic reversibility guarantees that it will always satisfy detailed balance.

The ME model that has been constructed can deal with the effects of molecular non-equilibrium on the reaction rates and with the preferential populations of states in the nascent products. Lack of experimental data preclude validation of the non-equilibrium aspects of the models but the predicted equilibrium rates are shown to agree well with the measured values over a wide temperature range.

Sample test flows have been presented for reacting flows in air. Comparisons with other computations show that within the shock layer, where the flow is being compressed, the flows are vibrationally cooler and less reactive than for the Bird models. This influences the transient levels of dissociation but not the final plateau values as the flow approaches equilibrium. Non-equilibrium products such as NO are significantly influenced and are predicted to be several times lower in concentration than by other codes.

The authors wish to acknowledge the helpful discussions with Professor Graeme Bird in developing the chemical reaction model. The research was supported by the Defence Research Agency through Agreement number AT/2037/331.

Appendix

In this study the set of 65 reactions proposed by Park (1990) was adopted. Among these reactions there are 30 that could be identified as atom exchange reactions and which can be modelled with the new method using the translational temperature as the controlling factor. The other reactions are controlled by the vibrational temperature. Table 2 gives the reactions that are included in the ME model with the controlling energy mode indicated, E_{vib} stands for the vibrational mode and E_{trans} for the translational.

Reaction	Energy mode
Dissociation reactions	
$N_2 + M \rightarrow N + N + M$	E_{vib}
$O_2 + M \rightarrow O + O + M$	E_{vib}
$NO + M \rightarrow N + O + M$	E_{vib}
$N_2^+ + e^- \rightarrow N + N$	E_{vib}
$O_2^+ + e^- \rightarrow O + O$	E_{vib}
Exchange reactions	
$NO + O \rightarrow N + O_2$	E_{vib}
$O_2 + N \rightarrow NO + O$	E_{trans}
$N_2 + O \rightarrow NO + N$	E_{vib}
$NO + N \rightarrow N_2 + O$	E_{trans}
Ionization reactions	
$N + O \rightarrow NO^+ + e^-$	E_{trans}
$N + N \rightarrow N_2^+ + e^-$	E_{trans}
$O + O \rightarrow O_2^+ + e^-$	E_{trans}
$O + e^- \rightarrow O^+ + e^- + e^-$	E_{trans}
$O^+ + e^- \rightarrow O + h\nu$	E_{trans}
$N + e^- \rightarrow N^+ + e^- + e^-$	E_{trans}
$N^+ + e^- \rightarrow N + h\nu$	E_{trans}
Charge exchange reactions	
$NO^+ + O \rightarrow N^+ + O_2$	E_{trans}
$O_2 + N^+ \rightarrow NO^+ + O$	E_{trans}
$N^+ + N_2 \rightarrow N_2^+ + N$	E_{trans}
$N + N_2^+ \rightarrow N_2 + N^+$	E_{trans}
$N + O_2^+ \rightarrow O_2 + N^+$	E_{trans}
$N^+ + O_2 \rightarrow O_2^+ + N$	E_{trans}
$O^+ + NO \rightarrow N^+ + O_2$	E_{trans}
$N^+ + O_2 \rightarrow O^+ + NO$	E_{trans}
$N_2 + O_2^+ \rightarrow O_2 + N_2^+$	E_{trans}
$O_2 + N_2^+ \rightarrow N_2 + O_2^+$	E_{trans}
$O + O_2^+ \rightarrow O^+ + O_2$	E_{trans}
$O^+ + O_2 \rightarrow O_2^+ + O$	E_{trans}
$NO^+ + N \rightarrow O^+ + N_2$	E_{trans}
$O^+ + N_2 \rightarrow NO^+ + N$	E_{trans}
$NO^+ + O_2 \rightarrow NO + O_2^+$	E_{trans}
$NO + O_2^+ \rightarrow NO^+ + O_2$	E_{trans}
$NO^+ + O \rightarrow O_2^+ + N$	E_{trans}
$O_2^+ + N \rightarrow NO^+ + O$	E_{trans}
$O^+ + N_2 \rightarrow N_2^+ + O$	E_{trans}
$N_2^+ + O \rightarrow O^+ + N_2$	E_{trans}
$NO^+ + N \rightarrow N_2^+ + O$	E_{trans}
$N_2^+ + O \rightarrow NO^+ + N$	E_{trans}

TABLE 2. Chemical reactions set (M in the dissociation reactions denotes any of the species of the flow)

REFERENCES

ALLEGRE, J. & BISCH, D. 1996*a* Experimental density flowfields over a 70° blunted cone at rarefied hypersonic conditions. In *Aerothermodynamics for Space Vehicles and High-Velocity Flow Data Base* (ed. W. Berry, J. Desideri, F. Grasso, J. Muylaert & J. Periaux). John Wiley & Sons. (In press.)

ALLEGRE, J. & BISCH, D. 1996*b* Heat transfer measurements over a 70° blunted cone at rarefied hypersonic conditions. In *Aerothermodynamics for Space Vehicles and High-Velocity Flow Data Base* (ed. W. Berry, J. Desideri, F. Grasso, J. Muylaert & J. Periaux). John Wiley & Sons. (In press.)

BIRD, G. A. 1981 Monte Carlo simulation in an engineering context. In *Rarefied Gas Dynamics, Progress in Aeronautics and Astronautics*, vol. 74 (ed. S. Fisher), pp. 239–255. AIAA.

BIRD, G. A. 1994 *Molecular Gas Dynamics and the Direct Simulation of Gas Flow*, Clarendon Press.

BORGNAKKE, C. & LARSEN, P. S. 1975 Statistical collision model for Monte Carlo simulation of polyatomic gas mixtures. *J. Comput. Phys.* **18**, 405–420.

CARLSON, A. B. & BIRD, G. A. 1995 Implementation of a vibrationally favoured dissociation method in DSMC. In *Rarefied Gas Dynamics 19, Proc. 19th Intl Symp. on Rarefied Gas Dynamics*. Oxford University Press.

CHAPMAN, S. & COWLING, T. G. 1972 *The Mathematical Theory of Non-uniform Gases*. Cambridge University Press.

GALLIS, M. A. & HARVEY, J. K. 1993 Application of the maximum entropy method to energy exchange, chemical reactions and ionisation in the simulation Monte Carlo method. *Imperial College AERO Rep.* 93 01. Imperial College, London.

HAAS, B. L. & BOYD, I. D. 1993 Models for direct Monte Carlo simulation of coupled vibration–dissociation. *Phys. Fluids* A **5**, 478–489.

HAAS, B. L., MCDONALD, L. D. & DAGUM, L. 1993 Models of thermal relaxation for particle simulation methods. *J. Comput. Phys.* **107**, 348–358.

KOURA, K. & MATSUMOTO, H. 1992 Variable soft sphere molecular model for inverse-power-law or Lennard Jones potentials. *Phys. Fluids* A **3**, 2459–2465.

LEVINE, R. D. & BERNSTEIN, R. B. 1987 *Molecular Reaction Dynamics and Chemical Reactivity*. Oxford University Press.

PARK, C. 1990 *Nonequilibrium Hypersonic Aerothermodynamics*. Wiley and Sons.

US Standard Atmosphere 1976 National Oceanic and Atmospheric Administration, National Aeronautics and Space Administration, United States Air Force.